Self-Organization in the Two-Dimensional Kelvin-Helmholtz Instability

Akira Miura

Department of Earth and Planetary Physics, University of Tokyo, Tokyo 113-0033, Japan
(Received 22 February 1999)

The evolution and relaxation of an initial shear flow subject to the Kelvin-Helmholtz instability are investigated via two-dimensional compressible hydrodynamic simulations and the calculus of variations. During the instability evolution the total kinetic energy remains almost constant, but the enstrophy decays rapidly by the selective dissipation with the artificial viscosity. The successive vortex pairings lead to the emergence of an isolated vortex and the initial shear flow relaxes toward a self-organized state, i.e., a nearly minimum enstrophy state in the incompressible fluid.

The Kelvin-Helmholtz (KH) instability excited by the velocity shear in fluid is a ubiquitously observed phenomenon in fluid dynamics. Although a real fluid is three dimensional (3D), the two-dimensional (2D) approximation of the flow is valid in many geophysical and astrophysical applications [1]. Therefore, the study of the 2D KH instability has been a subject of intensive experimental [2] and numerical [3] studies. In particular, the pairing of vortices appearing in the nonlinear stage of the KH instability [2] has been studied quite intensively because of its relevance to the observation of the emergence of ordered structures in the fully developed 2D shear layers for small Mach numbers [4] and for supersonic shear layers [5]. The purpose of this paper is to show by 2D compressible simulations for small Mach numbers that an initial shear flow subject to the KH instability evolves and relaxes by the successive pairings of vortices toward a self-organized state, i.e., a nearly minimum enstrophy state, which is obtained with the calculus of variations by assuming the constant total kinetic energy and the incompressibility. The self-organization in the continuous media in the present study [6] is the formation of ordered structure and specifically means the relaxation to the minimum enstrophy state [6].

The cascade of the turbulent flow to large scales owing to the enstrophy cascade to large wave numbers was shown numerically [7]. Numerical simulations of the 2D turbulent flows have also shown that isolated coherent vortices emerge in the turbulent flow by the merger of like-sign vortices [8]. The importance of the selective decay conjecture, i.e., the decay of the enstrophy while nearly conserving the total kinetic energy in the 2D turbulence, has been discussed [9]. The selective decay conjecture was confirmed by numerical simulations of 2D incompressible turbulence by calculating a sequence of the wave-number spectra of the total kinetic energy and the enstrophy [10]. In spite of these intensive studies on the 2D turbulence [1] of externally given vortices the nonlinear evolution of vortices spontaneously generated by the KH instability has not been studied from the point of self-organization [6]; the only exception is a recent experimental study using magnetized electron columns, which follow the same dynamics as 2D incompressible fluids, on the relaxation of 2D turbulence arising from the KH instability toward a meta equilibrium near the minimum enstrophy state [11].

The equation of fluid motion can be written as

$$\rho\left[\frac{\partial \mathbf{v}}{\partial t} + (\mathbf{v} \cdot \boldsymbol{\nabla})\mathbf{v}\right] = -\boldsymbol{\nabla}p + \eta\boldsymbol{\nabla}^2\mathbf{v}, \qquad (1)$$

where ρ, $\mathbf{v}$, and p are the mass density, the bulk velocity, and the pressure, respectively. The last term in the right-hand side (r.h.s.) of (1) represents the viscous dissipation due to the artificial viscosity, which is implicitly included in the numerical scheme [12]. For simplicity, let us assume that η is constant in space and time. From (1) we obtain the following general conservation equation of the enstrophy [13] in the 2D configuration:

$$\frac{\partial}{\partial t}\iint_C dx\,dy\,(\boldsymbol{\nabla} \times \mathbf{v})^2 = -\iint_C dx\,dy\,(\boldsymbol{\nabla} \times \mathbf{v})^2(\boldsymbol{\nabla} \cdot \mathbf{v}) + \iint_C dx\,dy\,[2(\boldsymbol{\nabla} \times \mathbf{v})] \cdot \frac{(\boldsymbol{\nabla}\rho \times \boldsymbol{\nabla}p)}{\rho^2}$$
$$- 2\nu\iint_C dx\,dy\,(\boldsymbol{\nabla} \times \boldsymbol{\Omega})^2 + 2\nu\iint_A [\boldsymbol{\Omega} \times (\boldsymbol{\nabla} \times \boldsymbol{\Omega})] \cdot d\mathbf{S}, \qquad (2)$$

where $\boldsymbol{\Omega} = \boldsymbol{\nabla} \times \mathbf{v}$, and $\nu = \eta/\rho$ is the kinematic viscosity. In (2), C represents a region in the x-y plane with $-x_b \leq x \leq x_b$ and $0 \leq y \leq L_y$, and A represents the surface surrounding the volume V, which consists of a region with $-x_b \leq x \leq x_b$, $0 \leq y \leq L_y$, and $0 \leq z \leq 1.0$. We assumed, as is also assumed in the following 2D simulations, that all physical quantities are inde-pendent of z and are periodic in the y direction, e.g., $\mathbf{v}(x, y = 0) = \mathbf{v}(x, y = L_y)$, and that v_x and derivatives with respect to x of the remaining quantities (ρ, v_y, p) vanish at $x = \pm x_b$.

A 2D simulation of the KH instability is performed in the x-y plane for an initial velocity profile of $v_{0y}(x) = (V_0/2)[1 - \tanh(x/a)]$ and for a convective sound Mach

number ($M_{SC} = 0.5V_0/C_S$) [14] equal to 0.25, where C_S is the sound speed. Time t is normalized by $2a/V_0$. For this configuration, the linearly fastest growing mode occurs at $2k_y a \sim 0.8$ with its growth rate equal to $0.17V_0/2a$ [15]. Therefore, the wavelength of the linearly fastest growing mode λ_{FGM} is nearly equal to $15.7a$. The length L_y of the periodic simulation box in the y direction is equal to $8 \times \lambda_{FGM} = 125.6a$ and we use $x_b = 40a$. A random incompressible velocity perturbation with its peak amplitude of v_x equal to $0.005V_0$ is given as an initial seed perturbation. A two-step Lax-Wendroff scheme is used in solving the ideal compressible hydrodynamic equations, and the number of grid points is equal to 400×400. The artificial viscosity ν in that scheme is given by $\nu \sim V_0^2 \Delta t/2$ [12], where Δt is the time step used in the simulation.

Figure 1 shows temporal evolutions of the total energy (dotted line), the total internal energy (dashed line), and the total kinetic energy (solid line) integrated in the whole simulation region. Each energy is normalized by $0.0628a^2 p_0$, where p_0 is the initial uniform pressure. The total kinetic energy remains almost constant during the simulation run. The difference of the total energy at $T = 600$ from the initial total energy is only 1% of the initial total energy.

Figure 2 shows temporal evolutions of the total square vorticity (enstrophy) integrated in the whole simulation region (solid curve), the contribution to the change of the total square vorticity due to the compressibility (dotted curve), and the baroclinic contribution [coming from the second term in the r.h.s. of (2)] to the change of the total square vorticity (dashed curve), which are normalized by V_0^2. After $T \sim 40$, the enstrophy decreases rapidly with time with a small oscillating component, which is due to the compressibility [coming from the first term in the r.h.s. of (2)]. Therefore, from Eq. (2) we conclude that the enstrophy, which is a global invariant in the 2D, inviscid, and incompressible fluid, decreases rapidly with

time due to the selective viscous dissipation [9] by the implicit artificial viscosity.

Figure 3 shows contour lines of the z component of the vorticity Ω_z at six different times from $T = 0$ to $T = 600$. In all panels the contour lines are plotted for negative vorticity (counterclockwise rotation). In the early phase an initial straight vorticity layer (velocity shear layer) develops into a vortex train at $T = 60$. Eight vortices appear as predicted by the linear theory. After $T = 60$, neighboring vortices begin to merge after counterclockwise rotation around each other. The successive pairings of vortices lead to the emergence of a single isolated vortex after $T = 400$.

Figure 4 shows the spectral amplitudes of the kinetic energy versus the wave number in the y direction at (a) $T = 0$ and (b) $T = 600$, and the spectral amplitudes of the enstrophy versus the wave number at (c) $T = 0$ and (d) $T = 600$. Each spectral amplitude is calculated by taking Fourier spectrum in the y direction at fixed x and then by taking the integral along x. The spectral amplitudes of the kinetic energy and the enstrophy are normalized by $2ap_0$ and $(V_0/2a)^2$, respectively. In this figure, k_{min} is the wave number equal to $k_{FGM}/8$, where $k_{FGM} = 2\pi/\lambda_{FGM}$. Figures 4(a) and 4(c) show that the spectral distributions of the kinetic energy and enstrophy at $T = 0$ are almost flat (nearly white noise). However, at $T = 600$, the spectral distributions of the kinetic energy and the enstrophy are well represented by power law distributions at $k/k_{min} < 70$. The spectral peak at $k = k_{min}$ at $T = 600$ of the kinetic energy occurs because of the inverse energy cascade. The power law exponents of the kinetic energy and the enstrophy at medium subrange of the wave number from $k/k_{min} = 10$ to 50 at $T = 600$ are equal to -3.50, which is close to the value obtained by Zabusky and Deem [3] and Lesieur et al. [3], and -1.35, respectively. This large difference of the power law exponents causes the selective enstrophy decay [9].
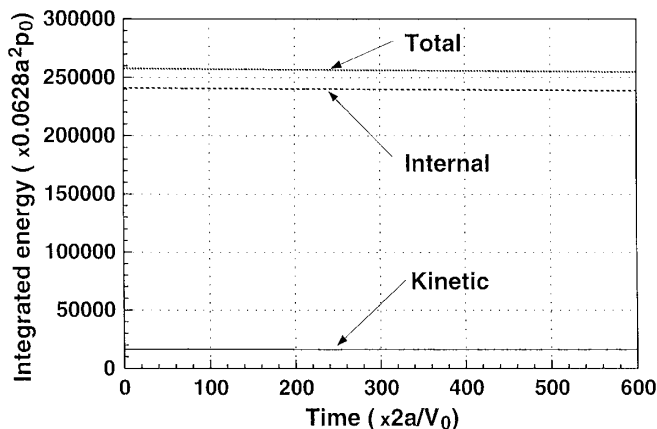
FIG. 1. Temporal evolutions of the total energy, the total internal energy, and the total kinetic energy integrated in the whole simulation region.
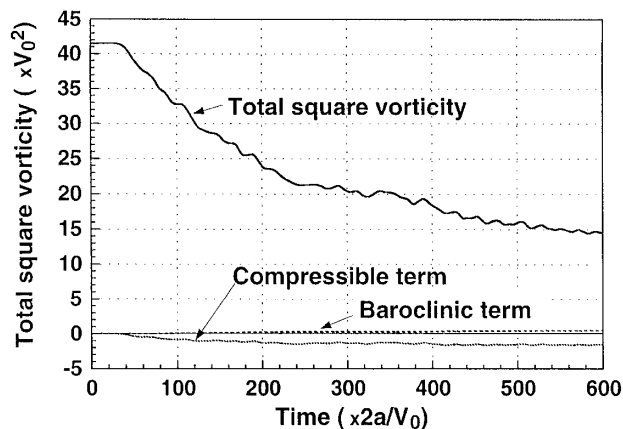
FIG. 2. Temporal evolutions of the total square vorticity (enstrophy), the contribution of the compressible term to the change of the total square vorticity, and the contribution of the baroclinic term to the change of the total square vorticity.
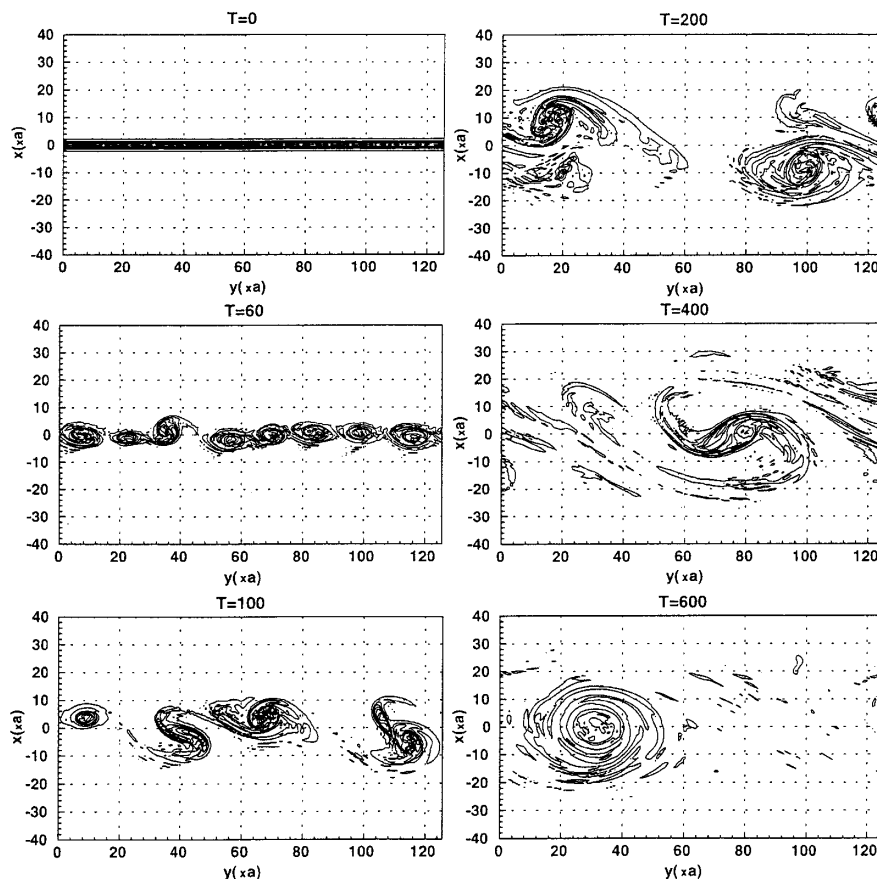
FIG. 3.   Temporal evolutions of the contours of the z component of the vorticity at six different times from $T = 0$ to $T = 600$.

The present results show that the total kinetic energy W remains relatively invariant, but the enstrophy U decays rapidly by the selective decay [9] during the evolution of the instability. Therefore, the appropriate variational principle describing the present self-organization is $\delta U - \lambda \delta W = 0$ [6]. By assuming the incompressibility (constant density) and using the boundary condition in the present simulation, this is reduced to the equation

$$\nabla \times \nabla \times \mathbf{v} = \lambda \mathbf{v}, \qquad (3)$$

which describes the minimum enstrophy state [6]. From (3) we obtain

$$\lambda = \frac{\int_C \Omega^2 \, dx \, dy}{\int_C v^2 \, dx \, dy}. \qquad (4)$$

By introducing the stream function $\psi(x, y)$, we obtain the eigenmode solution of (3) as

$$\psi(x, y) = \psi_0 \cos(k_x x) \sin(k_y y), \qquad (5)$$

with the eigenvalue

$$\lambda = k_x^2 + k_y^2, \qquad (6)$$

where ψ_0 is a constant. For the minimum λ or minimum enstrophy state, we obtain $k_x = \pi/(2x_b)$ and $k_y = 2\pi/L_y$. Therefore, the minimum eigenvalue $\lambda_{\min}$ obtained theoretically from (6) is equal to $0.00404/a^2$. On the other hand, by assuming that ρ is constant, we can cal-

culate λ from (4) by using values of the total kinetic energy and the total square vorticity obtained by simulations. At the final state $T = 600$ we obtain $\lambda_{\mathrm{sim}} = 0.00298/a^2$ from the simulation results. Simulation runs were also done for less compressible cases with $M_{\mathrm{SC}} = 0.125$ and 0.0625 and it was found that, for both cases, the selective decay occurred and the single isolated vortex appeared before $T = 600$. The Reynolds numbers R_e defined by the artificial viscosity as $R_e = 2aV_0/\nu$ are 128, 128, and 256 for $M_{\mathrm{SC}} = 0.25$, 0.125, and 0.0625, respectively. We obtained $\lambda_{\mathrm{sim}} = 0.00347/a^2$ and $0.00356/a^2$ at $T = 600$ for $M_{\mathrm{SC}} = 0.125$ and 0.0625, respectively. Therefore, λ_{sim} approaches $\lambda_{\min}$ as the Mach number decreases. Thus, the 2D vortices generated by the KH instability for small Mach numbers relax toward the nearly minimum enstrophy state in the incompressible fluid.

It is important to notice that vortex structures seen at $T = 60-600$ in Fig. 3 in the present nonequilibrium system with flow seem to be dissipative structures emerging in nonequilibrium open systems [16], because the local region surrounding each vortex is open to the flow from outside, although the whole simulation system is periodic and is not an open system.

In summary, the observed irreversible relaxation of the initial shear flow subject to the KH instability toward a nearly minimum enstrophy state by the selective decay presents evidence that the successive pairings of vortices
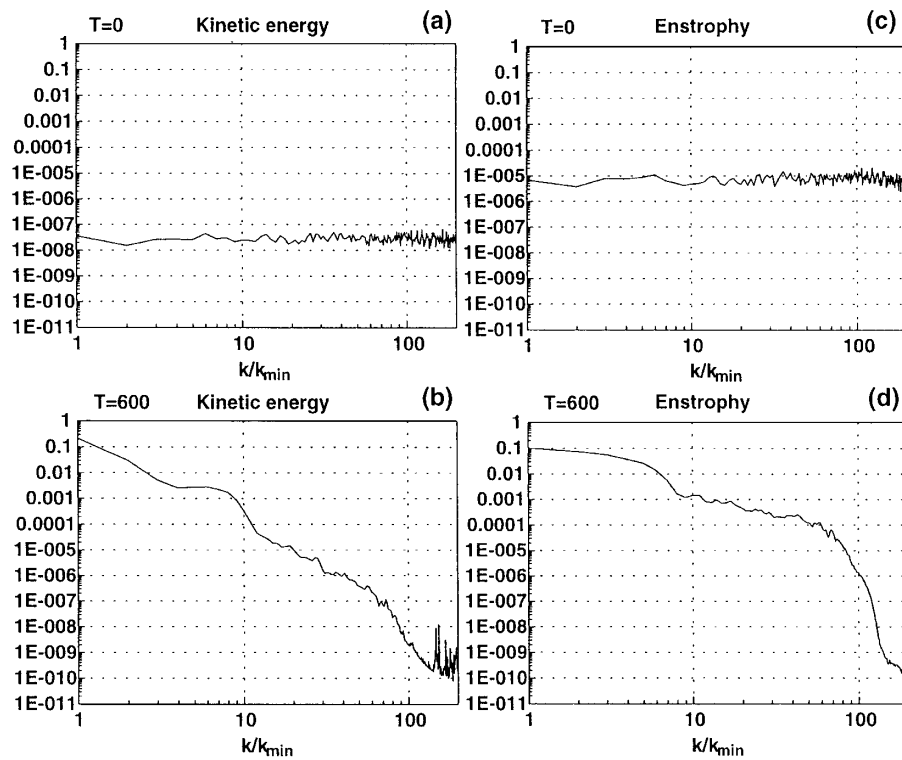
FIG. 4. The spectral amplitudes of the kinetic energy versus the wave number in the y direction at (a) $T = 0$ and (b) $T = 600$. The spectral amplitudes of the enstrophy versus the wave number at (c) $T = 0$ and (d) $T = 600$.

occurring in the nonlinear stage of the 2D KH instability is a self-organization process [6]. This indicates that, although the KH instability is essentially an inviscid phenomenon, the self-organization or the successive pairings of vortices in the nonlinear stage occurs due to the presence of a finite viscosity, which leads to the selective decay of the enstrophy.

[1] R. H. Kraichnan and D. Montgomery, Rep. Prog. Phys. **43**, 547 (1980); U. Frisch, *Turbulence* (Cambridge University Press, Cambridge, England, 1995).

[2] C. D. Winant and F. K. Browand, J. Fluid Mech. **63**, 237 (1974); F. K. Browand and P. D. Weidman, J. Fluid Mech. **76**, 127 (1976); C.-M. Ho and L.-S. Huang, J. Fluid Mech. **119**, 443 (1982).

[3] N. J. Zabusky and G. S. Deem, J. Fluid Mech. **47**, 353 (1971); P. C. Patnaik, F. S. Sherman, and G. M. Corcos, J. Fluid Mech. **73**, 215 (1976); G. M. Corcos and F. S. Sherman, J. Fluid Mech. **139**, 29 (1984); R. W. Metcalfe, S. A. Orszag, M. E. Brachet, S. Menon, and J. J. Riley, J. Fluid Mech. **184**, 207 (1987); M. Lesieur, C. Staquet, P. Le Roy, and P. Comte, J. Fluid Mech. **192**, 511 (1988); S. K. Lele, in Proceedings of the 27th Aerospace Science Meeting, AIAA-89-0374, Reno, Nevada, 1989 (unpublished).

[4] G. L. Brown and A. Roshko, J. Fluid Mech. **64**, 775 (1974).

[5] D. Papamoschou and A. Roshko, J. Fluid Mech. **197**, 453 (1988).

[6] A. Hasegawa, Adv. Phys. **34**, 1 (1985).

[7] P. Rhines, J. Fluid Mech. **69**, 417 (1975).

[8] J. C. McWilliams, J. Fluid Mech. **146**, 21 (1984).

[9] F. P. Bretherton and D. B. Haidvogel, J. Fluid Mech. **78**, 129 (1976); W. H. Matthaeus and D. Montgomery, Ann. N.Y. Acad. Sci. **357**, 203 (1980); C. E. Leith, Phys. Fluids **27**, 1388 (1984).

[10] W. H. Matthaeus, W. T. Stribling, D. Martinez, S. Oughton, and D. Montgomery, Phys. Rev. Lett. **66**, 2731 (1991).

[11] X.-P. Huang and C. F. Driscoll, Phys. Rev. Lett. **72**, 2187 (1994); X.-P. Huang, K. S. Fine, and C. F. Driscoll, Phys. Rev. Lett. **74**, 24 (1995); K. S. Fine, A. C. Cass, W. G. Flynn, and C. F. Driscoll, Phys. Rev. Lett. **75**, 3277 (1995).

[12] R. D. Richtmyer and K. W. Morton, *Difference Methods for Initial Value Problems* (Wiley-Interscience, New York, 1967), 2nd ed.

[13] A. Miura, Phys. Plasmas **4**, 2871 (1997); A. Miura, J. Geophys. Res. **104**, 395 (1999).

[14] D. Papamashou and A. Roshko, J. Fluid Mech. **197**, 453 (1988).

[15] A. Miura and P. L. Pritchett, J. Geophys. Res. **87**, 7431 (1982).

[16] G. Nicolis and I. Prigogine, *Self-Organization in Nonequilibrium Systems: From Dissipative Structures to Order Through Fluctuations* (Wiley, New York, 1977).